# Geometric consideration of nanostructures for energy storage systems

J. Park,[1,a)] J. Li,[1] W. Lu,[2] and A. M. Sastry[3]
[1]*Department of Mechanical and Aerospace Engineering, Missouri University of Science and Technology, Rolla, Missouri 65401, USA*
[2]*Department of Mechanical Engineering, University of Michigan, Ann Arbor, Michigan 48109, USA*
[3]*Sakti3, Inc., Ann Arbor, Michigan 48108, USA*

(Received 29 October 2015; accepted 19 December 2015; published online 8 January 2016)

Battery performance and its fade are determined by various aspects such as the transport of ions and electrons through heterogeneous internal structures; kinetic reactions at the interfaces; and the corresponding interplay between mechanical, chemical, and thermal responses. The fundamental factor determining this complex multiscale and multiphysical nature of a battery is the geometry of active materials. In this work, we systematically consider the tradeoffs among a selection of limiting geometries of media designed to store ions or other species via a diffusion process. Specifically, we begin the investigation by considering diffusion in spheres, rods, and plates at the particle level, in order to assess the effects of geometry, diffusivity, and rate on capacity. Then, the study is extended to considering of the volume fraction and particle network, as well as kinetics at the interface with electrolyte. Our study suggests that, in terms of overall bulk level material performance, thin film batteries may generate the highest energy density with high power capability when they are implemented at nanoscales or with highly diffusion materials. © *2016 AIP Publishing LLC*.
[http://dx.doi.org/10.1063/1.4939282]

## I. INTRODUCTION

Many reactions and processes in diverse applications rely on the transfer of mass within a solid, a liquid, and a gas. In energy storage/generation systems, such as batteries, supercapacitors, and fuel-cells, the transport of the species determines the key physics inside the systems because they operate by transporting electrons and ions through heterogeneous materials.[1–3] For instance, in battery systems, the ions travel between the electrodes and the electrolyte, while electrons flow in the electrodes only. Generally, the electrons move much faster than the ions and, thus, transport of the ions is a limiting factor for the process. This limiting factor is one of the main obstacles to further improvement of the system's performance. For instance, the key requirement in modern energy storage systems to assure clean vehicles, clean energy, and portable devices is high energy/power density. Power density is limited by the speed of the species being transported.

Energy density, however, is another matter. This is related to how much of the energy carrying species are stored inside the materials, as measured by the capacity. Theoretical capacity is generally assumed to be an intrinsic property. However, capacity *utilization* is affected by the species transport process. The common metaphor of a highway traffic bottleneck applies, wherein a locally high concentration of cars prevents the entire highway from accommodating the largest number of cars possible, because of excluded areas. Thus, as in the metaphor, the species' diffusivity is a key factor that must be considered in the initial design stage of a system in order to achieve specific goals.

The high demand for energy and power density in modern batteries has provoked intense study of the utilization of various nanostructures in electrodes, since they have been presumed to offer intrinsic benefits such as short diffusion lengths, large surface areas, and enhanced ionic and electronic conductivities.[4–15] Practical challenges related to the integration of these nanostructures, such as high fabrication cost (due to the complex synthetic process) and low volumetric energy density (due to reduced packing density), have contributed to slow adoption. Also, nanostructured electrodes are prone to undesired side reactions because of the large surface area that is exposed to the electrolyte. Further, nanomaterials tend to form agglomerates during fabrication that lead to the loss of intrinsic characteristics of the nanostructures.

Thus, the theoretical benefits of these materials, so far, have not been achieved in many practical systems due to high intrinsic costs (for all of the reasons above) for their integration into practical devices. Thus, in light of the challenges to their integration, the potential benefits of these materials appear to be a reasonable pursuit. In particular, diffusion is a limiting factor with regard to a charge transfer reaction in high power applications. This high power is one of the significant benefits of the nanostructured electrode systems, so the diffusion-limiting process becomes more vital in those systems.[16] Thus, in this work, we endeavored to provide general comparisons between three representative nanostructures, with a focus on the particle geometry and corresponding transport process.

We began with the solid-phase diffusion-limiting process in the simplest structures. We selected three of the structures—1D thin films, 2D nanowires, and 3D spheres. This distinction was based on the diffusion process. For instance, nanowire, nanotube, and nanopilar are generally considered to be 1D-structures, but the species flow have to be considered as a 2D-configuration as shown in Fig. 1. Accordingly, 1D-nanostructures include thin films, nanodisks, and nanosheets. Nanoparticles, nanospheres, and nanoflowers belong to 3D-structures.

[a)]parkjonghy@mst.edu.

 

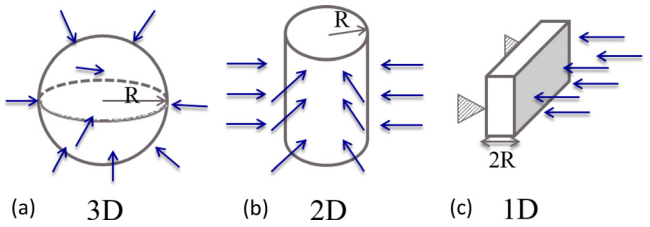


FIG. 1. Selected three representative structures and their idealized configurations: (a) 3D sphere, (b) 2D cylinder, and (c) 1D thin film.

Generally, the 2D and 3D particles are used as forms of porous electrode structures to increase the areal energy density and specific surface area. In this case, the packing methodologies affecting the volume fraction and tortuosity have to be considered so as to identify the geometry impact on battery performance. In order to investigate and determine the effect of this volume fraction, we extended single particle results to packing geometry.

An analysis based on the diffusion-limiting process with the idealized geometry may provide useful information on the geometric selection for nanostructured energy storage systems. The concentration of the ions in electrolyte around the solid-phase, however, is needed to determine the kinetics associated with the reaction between the solid and electrolyte at the interface. This means that a diffusion-only model of the ions in the solid particle is not sufficient to capture the exact phenomena between the particle and the electrolyte at the interface. Finally, we confirmed the results from an analysis of a diffusion-limiting case by considering the ions' dissociation from or reduction into the active materials in the realistic composite electrodes during the discharge-charge processes. These consecutive investigations via different models from the particle level to the cell level, and also from the simple diffusion process to complex kinetic reaction, provided us with a clear understanding of the relation between the electrode geometry and its system performance.

## II. METHOD

As described earlier, the key physics determining the performance of energy storage systems is the diffusion process in solid phases. In order to analyze the diffusional behavior in a single particle, three idealized geometries were selected, as shown in Fig. 1. Homogeneous structures were assumed with a linear diffusion process. A constant flux boundary condition was considered and a specific battery system was chosen in order to demonstrate a case. Table I shows the key parameters for the experiments that focused on the battery system. A lithium manganese oxide (LMO) material was selected to represent the battery materials. Three particle sizes (0.1, 1, 10 $\mu$m) were considered for observation of the size effect. The base line diffusivity was selected as $D_{LMO}$ ($7.08 \times 10^{-15}$ m$^2$/s) from Ref. 17. By considering the theoretical density of the material, the maximum concentration of the species ($C_{max}$) was assigned as 22 900 mol/m$^3$.

The diffusion equations corresponding to each case are supplied in Table II. Also, the corresponding boundary conditions are expressed as a form of the Neumann boundary

TABLE I. Experimental parameters.

| | Variables | Notes |
|---|---|---|
| Particle size ($R$, $\mu$m) | 0.1, 1, 10 | |
| $C_{rate}$ | 0.1, 1, 10 | Evaluated based on the maximum concentration |
| Diffusivity ($D$, m$^2$/s) | $D_{LMO}$ 10 × $D_{LMO}$ | Constant diffusivity was assumed |
| $C_{max}$ (mol/m$^3$) | 22 990 | Density: 4140 m$^3$/kg |

condition, as shown in Table II. Here, $c$ (mol/m$^3$) is the concentration of the diffusing substance, $D$ (m$^2$/s) is diffusivity, $r$ and $z$ are the spatial coordinates in the spherical, circular, and axial coordinate, respectively, $t$ (s) is time, and $I_d$ is the flux (mol/m$^2$/s). The flux can be expressed by $C_{rate}$, which is used to scale the charge or discharge current of a battery ($x$ $C_{rate}$ means that a charge or a discharge is done for $1/x$ hour), based on the following relationship:

$$\int_0^{\frac{3600}{C_{rate}}} \left( \int I_d ds \right) dt = C_{\max} \times V, \tag{1}$$

where $V$(m$^3$) is the total volume of the particle. As a result, the flux for each case is obtained as follows:

$$I_d = \frac{C_{rate}}{3} \frac{C_{\max}}{3600} R\,(3D), \quad I_d = \frac{C_{rate}}{2} \frac{C_{\max}}{3600} R\,(2D), \quad \text{and } I_d = \frac{2C_{rate}}{1} \frac{C_{\max}}{3600} R\,(1D). \tag{2}$$

Even though this simple analysis based on the diffusion-limiting case can provide a clear understanding regarding the geometry-dependent battery performance, the battery responses are also affected by several other key physics, such as interface reactions between the solid and electrolyte phases and transportation in the electrolyte phase. Next, in order to consider the kinetic reaction at the interface between the solid materials and electrolyte in a porous composite electrode, an electrochemical model was developed. At the interface between the active material and the electrolyte, lithium ions are dissociated from or reduced into $Li_xMn_2O_4$ during the discharge-charge processes as

$$Li_{1-x}Mn_2O_4 + xLi^+ + xe^- \underset{charge}{\overset{discharge}{\rightleftharpoons}} LiMn_2O_4. \tag{3}$$

TABLE II. Governing equations and the corresponding boundary conditions.

| Dimension | Geometry | Governing Eq. | B.C.s |
|---|---|---|---|
| 3D | 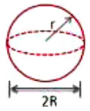 | $\frac{\partial c}{\partial t} = \frac{D}{r^2}\frac{\partial}{\partial r}\left(r^2 \frac{\partial c}{\partial r}\right)$ | $\frac{\partial c}{\partial r}\Big\|_{r=0} = 0, \frac{\partial c}{\partial r}\Big\|_{r=R} = -\frac{I_d}{D}$ |
| 2D | 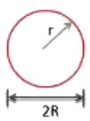 | $\frac{\partial c}{\partial t} = \frac{D}{r}\frac{\partial}{\partial r}\left(r \frac{\partial c}{\partial r}\right)$ | $\frac{\partial c}{\partial r}\Big\|_{r=0} = 0, \frac{\partial c}{\partial r}\Big\|_{r=R} = -\frac{I_d}{D}$ |
| 1D |  | $\frac{\partial c}{\partial t} = Dr\frac{\partial^2 c}{\partial z^2}$ | $\frac{\partial c}{\partial z}\Big\|_{r=0} = 0, \frac{\partial c}{\partial z}\Big\|_{z=R} = -\frac{I_d}{D}$ |

The rate of the reactions represented by Eq. (3) can be modeled by the Butler-Volmer equation

$$j^{Li} = i_0\left[\exp\left(\frac{\alpha_a F}{RT}\eta\right) - \exp\left(-\frac{\alpha_c F}{RT}\eta\right)\right], \tag{4}$$

where $i_0$ is the exchange current density, $\alpha_a, \alpha_c$ are anodic and cathodic transfer coefficients for the electrode, respectively, $R$ is the gas constant, $F$ is the Faraday's constant, and $T$ is the temperature. Here, $\eta$ stands for the surface overpotential defined as

$$\eta = \phi_s - \phi_e - U, \tag{5}$$

where $\phi_s, \phi_e$ are the surface potentials at the interface of the electrode and the electrolyte, and $U$ is the open circuit potential. The exchange current density determines the rate of the reaction and depends upon the reactant and product concentration adjacent to the interface as follows:

$$i_0 = k(c_s)^{\alpha_c}(c_s^{\max} - c_s)^{\alpha_a}(c_e)^{\alpha_a}, \tag{6}$$

where $c_s$ and $c_e$ represent Li-ion concentration at the particle surface and in the electrolyte, $c_s^{\max}$ stands for the maximum surface concentration, and $k$ is the reaction rate constant.

The governing equations for the electrodes and the electrolyte involve charge conservation in the solid (Eq. 7) and the electrolyte (Eq. 8), and mass transport law in the solid (Eq. 9) and the electrolyte (Eq. 10)

$$\nabla\cdot(\sigma\nabla\phi_s) = 0, \tag{7}$$

$$\nabla\cdot\left(-\kappa\nabla\phi_e - \frac{\kappa RT}{F}\left(1+\frac{\partial \ln f}{\partial \ln c_e}\right)\left(1-t_+^0\right)\nabla\ln c_e\right) = 0, \tag{8}$$

$$\frac{\partial c_s}{\partial t} + \nabla\cdot(-D_s\nabla c_s) = 0, \tag{9}$$

$$\frac{\partial c_e}{\partial t} + \nabla\cdot(-D_e\nabla c_e) + \frac{\mathbf{i}\cdot\nabla t_+^0}{F} = 0, \tag{10}$$

where $\sigma$ is the conductivity of the solid particle, $\kappa$ is ionic conductivity in the electrolyte, $f$ is the mean molar activity coefficient, $t_+^0$ is the cation transference number, $D_s$ is the diffusion coefficient in the solid, $D_e$ is the diffusion coefficient in the electrolyte, and $\mathbf{i}$ is the current density in the electrolytic solution.

## III. RESULTS AND DISCUSSIONS

Fig. 2 shows relative capacity changes, depending on geometry and $C_{rate}$ for base diffusivity from the three simple geometries shown in Fig. 1. The blue square lines are from the 1D-structures, the green star lines are from the 2D-structures, and the red diamond lines are from the 3D-structures. Our first observation was that, as the particle size increased, the capacity decreased due to the diffusion-limiting process. Especially, when the $C_{rate}$ was high for large particles, the capacity utilization became very poor. The delayed diffusion process, caused by the longer diffusion path inside the large particles, caused an accumulation of species on the surfaces of the particles.

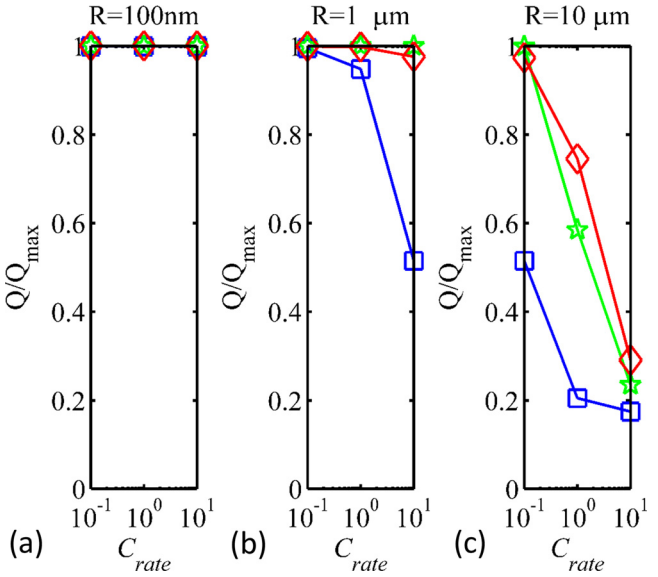


FIG. 2. Relative capacity change depending on geometry and $C_{rate}$ for base diffusivity ($D_{LMO}$): blue-square (1D), green-star (2D), red-diamond (3D): (a) R = 100 nm, (b) R = 1 $\mu$m, and (c) R = 10 $\mu$m.

This phenomenon became intense when the $C_{rate}$ was high, so the concentrations on the particle surfaces reached the maximum values quickly, which ceased further intercalation processes. The specific areas of each structure were 3/R, 2/R, 1/R from 3D to 1D, respectively; thus, the power capability of 3D was highest. However, as the particle size decreased into nanoscales, the performances were almost identical, regardless of the $C_{rate}$ and particle geometry. In nanostructures, due to the short diffusion length, power capability was not a limiting factor. Similarly, the $C_{rate}$ had less effect on the capacity utilization at nanoscale. This can be confirmed from the first figure where R = 100 nm.

Diffusivity is another important factor in determining the capacity utilization. Fig. 3 shows the effect of diffusivity.

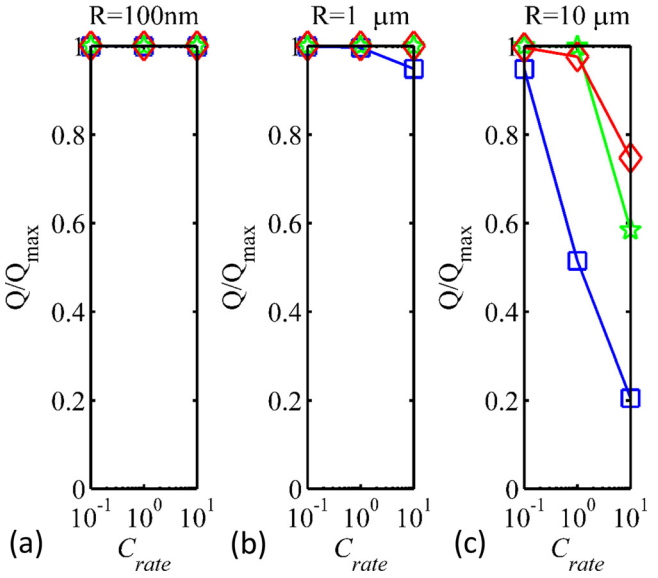


FIG. 3. Relative capacity change depending on geometry and $C_{rate}$ with an increased diffusivity ($10\times D_{LMO}$): blue-square (1D), green-star (2D), red-diamond (3D): (a) R = 100 nm, (b) R = 1 $\mu$m, and (c) R = 10 $\mu$m.

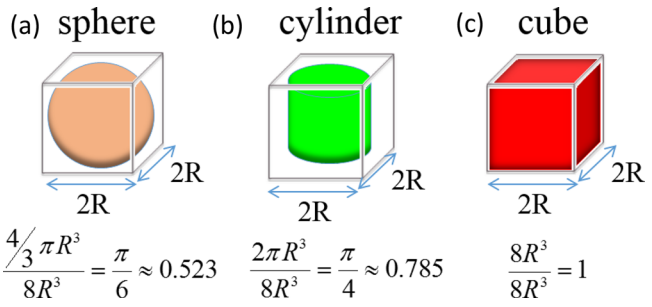


FIG. 4. Relative volume fractions to a cube for three geometries: (a) Sphere, (b) Cylinder, and (c) Cube.

Generally, as the diffusivity increases, the capacity utilization also increases because the enhanced diffusivity allows more ions to flow in easily. A normalized diffusion parameter is $(L^2 \times t)/D$, which indicates that $x$ times increased diffusion coefficient is equivalent to $\sqrt{x}$ times reduction in the diffusion path. For instance, the case with R = 10 $\mu$m with $10 \times D_{LMO}$ (shown in Fig. 3) is expected to be similar to the case of middle of R = 1 $\mu$m and R = 10 $\mu$m with $D_{LMO}$ (shown in Fig. 2). In summary, the capacity utilization of nanosized structures, or some materials with highly improved diffusivity, is not significantly affected by the geometry.

However, practically, we needed to consider bulk materials because real systems are generally at that scale. The volume fraction of particles varies depending on geometry. The volume fractions of each individual particle (3D sphere, 2D cylinder, and 1D film), relative to a cubic, were $\pi/6$, $\pi/4$, and 1, respectively, as shown in Fig. 4. The 1D film shows the highest value and the 3D sphere shows the lowest value. Fig. 5 shows the relative capacity density by considering the volume fraction (shown in Fig. 4). Due to the low volume fraction of the 3D sphere, it shows the lowest energy density for nanosized particles.

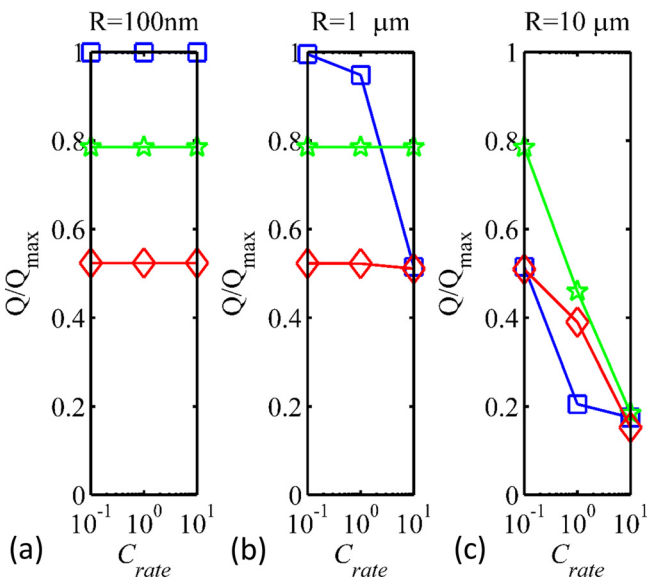


FIG. 5. Relative capacity by considering volume fraction: blue-square (1D), green-star (2D), red-diamond (3D): (a) R = 100 nm, (b) R = 1 $\mu$m, and (c) R = 10 $\mu$m.

TABLE III. Packing density of ordered spheres.

| Spheres | Volume fraction |
|---|---|
| Hlose packed | 0.74 |
| Tetrahedral lattice | 0.34 |
| Cubic lattice | 0.52 |
| Hexagonal lattice | 0.60 |

When we consider multiple particles, the packing density is directly related to the energy density. The packing fraction of particles depends on their geometries and the packing method (ordered or disordered). For ordered 3D spherical particle structures, the packing density varies from 0.34 to 0.74,[18–21] as shown in Table III. The tetrahedral lattice shows the minimum and the close packing shows the highest value. For the random packing, a Monte Carlo simulation (called "mechanical contraction") demonstrated that the density of randomly packed spherical particles was 0.631.[22,23] For the 2D-structures, the maximum packing density is 0.9 when the rods are closely packed, and the packing density is 0.4 when the rods are packed with a gap of one radius between the particles (as shown in Fig. 6). For the randomly packed 2D-rods, several independent theoretical and experimental studies led to a similar estimation, 0.84.[24,25] The packing density of the closely packed 1D-structures is 1.

Fig. 7 shows the range of capacity change by considering the packing density. When the particle size was around 100 nm, the 1D thin film shaped structures showed the maximum capacity, even in a high $C_{rate}$. However, when the particle size became around 10 $\mu$m, 2D or 3D structures showed a higher capacity than the 1D thin film, depending on the packing density. For the sizes around 1 $\mu$m, thin film showed a better performance with a lower $C_{rate}$, but it was worse with a high $C_{rate}$.

The correlation between capacity utilization, diffusivity, particle size, particle geometry, and the current density can be interpreted by comparing analytical solutions of the governing equations for 1D and 3D (shown in Table II) with a simple boundary condition.[26] For this demonstration, we considered a case in which the initial concentration was zero, and the surfaces of the particles approached an equilibrium concentration of $C_0$, exponentially, i.e., $C_0(1 - \exp(-\beta t))$. This represented a surface concentration that changed rapidly, but not

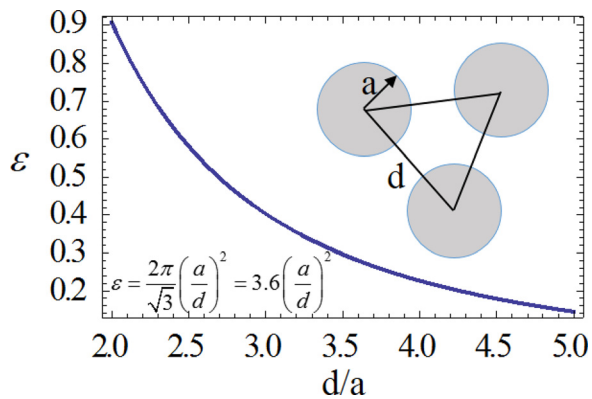


FIG. 6. Volume fraction of 2D structures depending on packing.

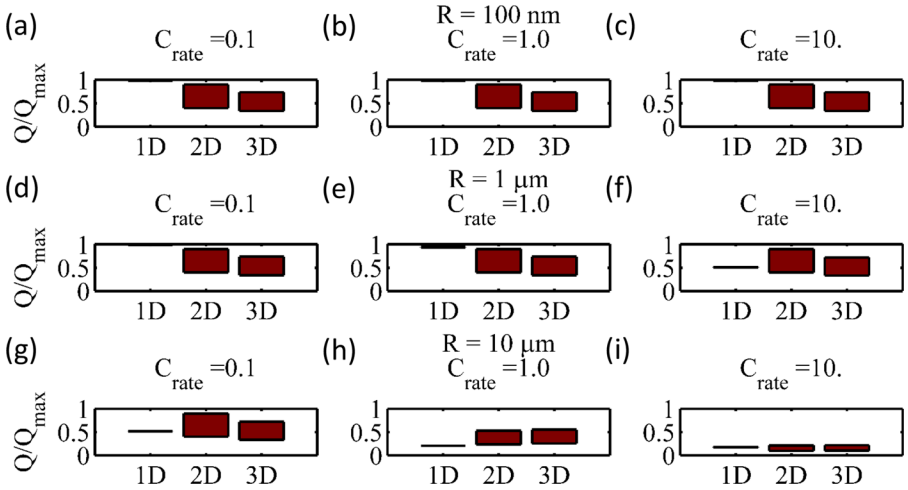


FIG. 7. Ranges of relative capacity by considering the packing density: (a) $R = 100\,nm$ $C_{rate} = 0.1$, (b) $R = 100\,nm$ $C_{rate} = 1$, (c) $R = 100\,nm$ $C_{rate} = 10$, (d) $R = 1\,\mu m$ $C_{rate} = 0.1$, (e) $R = 1\,\mu m$ $C_{rate} = 1$, (f) $R = 1\,\mu m$ $C_{rate} = 10$, (g) $R = 10\,\mu m$ $C_{rate} = 0.1$, (h) $R = 10\,\mu m$ $C_{rate} = 1$, and (i) $R = 10\,\mu m$ $C_{rate} = 10$.

instantaneously. The concentration of the diffusional species can be obtained by solving the diffusion equations in Table II with the equilibrium concentration condition at the surface boundary. The corresponding relative capacities to the maximum value are given for 1D and 3D structures, respectively,

$$Q/Q_{\max} = 1 - \exp(-\beta t)\frac{\tan\lambda}{\lambda^{1/2}} - \frac{8}{\pi^2}\sum_{n=0}^{\infty}\frac{\exp\left[-(2n+1)^2\left(\pi Dt/4R^2\right)\right]}{(2n+1)^2\left[1-(2n+1)^2(\lambda\pi^2/4)\right]}, \tag{11}$$

$$Q/Q_{\max} = 1 - \frac{3}{\lambda}\exp(-\beta t)\{1-\lambda^{1/2}\cot\lambda^{1/2}\} + \frac{6\lambda}{\pi^2}\sum_{n=0}^{\infty}\frac{\exp\left[-Dn^2\pi^2 t/R^2\right]}{n^2[n^2\pi^2-\lambda]}, \tag{12}$$

where $\lambda = \beta R^2/D$, and R represents the size of film and sphere and $\beta$ indicates the rate of flux. Consequently, a lower $\lambda$ represents a small particle or a high diffusivity or a low $C_{rate}$. Fig. 8 shows the total amount of diffusing substance in the particles, which was normalized with respect to maximum concentration. As seen in Fig. 8, the total amounts of diffusing substance in the film and sphere were very similar for a lower $\lambda$, which is consistent with Figs. 2 and 3. However, for a larger $\lambda$ representing large particles or a low diffusivity or a high $C_{rate}$, the discrepancy between them increased, as we also observed.

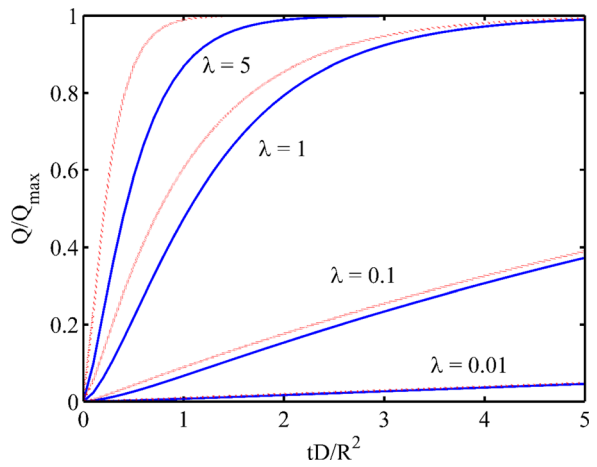


FIG. 8. Relative amount of diffusing substance for surface concentration given by $C_0(1-\exp(-\beta t))$. Numbers on curves are values of $\lambda = \beta R^2/D$. Red dotted lines are for spheres and blue solid lines are for thin film.

In addition, the observed phenomena can be interpreted with the aid of an impedance analysis. In nanostructure electrodes, due to the short diffusion length, the diffusing substances quickly reach the center of a spherical particle or impermeable substrate. As a result, they show different features in diffusion impedance; a capacitive behavior, rather than the original Warburg behavior, showing increased solid-phase diffusion impedance as the frequency decreases.[27] Also, the size-dependent impedance was confirmed from a recent experiment that compared the measured impedances from electrodes of 15, 35, and 55 $\mu$m particles and found that the smallest powder anodes had the lowest resistance.[28]

In order to confirm the results from the diffusion-limiting analysis, the developed electrochemical model (shown in Section II) was utilized. This model includes the kinetic reaction between the electrolyte and solid phase at the interface, as well as the particle network of the composite electrodes. It is a two-dimensional electrochemical model. For simplicity, two extreme cases of thin film electrode and composite electrode of spherical particles were compared. For the composite electrode, the particles were randomly located under a given volume fraction; three cases were considered: 0.7, 0.5, and 0.35. The average of values, from three independent cases, was considered for final analysis. Fig. 9 shows the calculated capacity from the electrochemical model with different porosity. One clear observation of the previous diffusion-limiting case was a capacity decrease with an increase of the electrode thickness. Delayed diffusional process through the long path in the solid phase caused the capacity decrease. Another observation was that capacity decrease became severe as the $C_{rate}$ increased. Especially, the decrease became worse for the thin film case. This is the same result obtained from the diffusion-limiting case, as shown in Fig. 2. The smaller specific area limited the power performance for thick thin film electrodes when

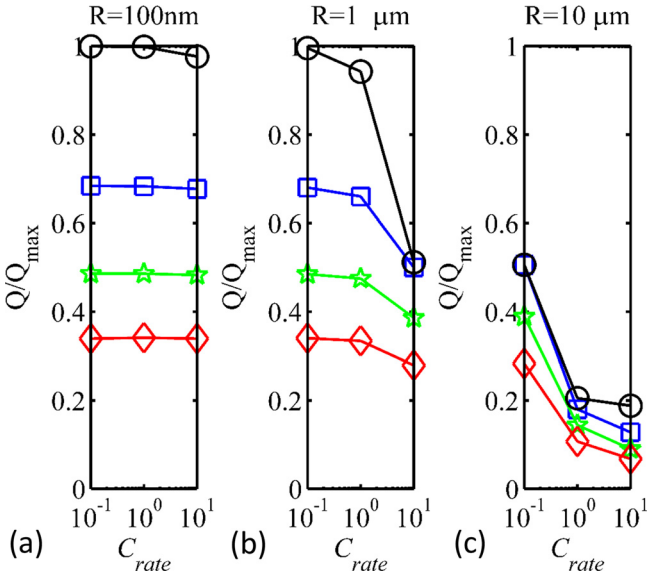


FIG. 9. Relative capacity from the electrochemical model: blue-square (30% porosity), green-star (50% porosity), red-diamond (65% porosity), black-sphere (thin film): (a) R = 100 nm, (b) R = 1 $\mu$m, and (c) R = 10 $\mu$m.

the $C_{rate}$ was high. When compared with the diffusion-limiting case (Fig. 2), the composite electrode showed lower capacity. This may have been due to the particle network. Capacity was determined by the local transport of ions and electrons through inhomogeneous internal structures and the kinetic reactions at the interfaces among them. These spatial inhomogeneities generated localized fluxes and irregular gradients of species concentration and, eventually, different cell capacity. Despite some deviation in the capacity itself, in general, the conclusions from the diffusion-limiting analysis were valid for real battery systems.

The current analysis that focused on the diffusion-limiting case gave us an important insight into the effects of geometry on battery capacity. Especially, when the system is more focused on high power applications, the diffusion-limiting process will become more important, and findings from this work can be more meaningful. This model can be applied from the early design status to decisions for selecting a fundamental geometry of the system. This finding has important implications for a variety of systems and, most particularly, battery systems. To date, battery systems have shown a wide range of selections in terms of diffusivity (Cathode: $10^{-8}$–$10^{-15}$ cm$^2$/s from $LiCoO_2$, $LiMn_2O_4$, and $LiFePO_4$, Anode: $10^{-9}$–$10^{-13}$ cm$^2$/s from graphite, germanium, and silicon) and film dimensions (1–100 $\mu$m) for different target rates (e.g., 10–20 C for Hybrid Electric Vehicles and 5 C for Electric Vehicles).[29–35]

## IV. CONCLUSIONS

We simply, but systematically, studied the relationship between the capacity utilization and geometry of a diffusion system. Specifically, consideration was given to the diffusion process for spheres, rods, and plates as the model structures with bulk material characteristics, and packing densities, in order to assess the rate effects and total capacities at bulk material levels. It was concluded that 1D–structures, i.e., thin films, when implemented at nanoscales, or with highly diffusive materials, can be expected to generate the highest energy density with high power capability. By validating these conclusions, the finding from this work is expected to be a practical guidance for the design of energy storage systems, especially, for the nanostructured electrode systems.

## ACKNOWLEDGMENTS

The authors acknowledge the support of this project provided by the General Motors/University of Michigan Advanced Battery Coalition for Drivetrains, with additional sponsorship by Materials Research Center at Missouri University of Science and Technology.

[1]P. M. Panchmatia *et al.*, "Lithium-ion diffusion mechanisms in the battery anode material $Li_{1+x}V_{1-x}O_2$," Phys. Chem. Chem. Phys. **16**(39), 21114–21118 (2014).
[2]L. Mai *et al.*, "Fast ionic diffusion-enabled nanoflake electrode by spontaneous electrochemical pre-intercalation for high-performance supercapacitor," Sci. Rep. **3**, 1718 (2013).
[3]S. Latorrata *et al.*, "Design of properties and performances of innovative gas diffusion media for polymer electrolyte membrane fuel cells," Prog. Org. Coat. **78**(0), 517–525 (2015).
[4]Q. He *et al.*, "A novel mesoporous carbon@silicon-silica nanostructure for high-performance Li-ion battery anodes," Chem. Commun. **50**(90), 13944–13947 (2014).
[5]B.-S. Lee *et al.*, "Novel multi-layered 1-D nanostructure exhibiting the theoretical capacity of silicon for a super-enhanced lithium-ion battery," Nanoscale **6**(11), 5989–5998 (2014).
[6]X. Lin *et al.*, *Noble Metal Nanostructure for Use in Solar Battery Surface, Comprises N-Type Aluminum Indium Phosphate Layer on Upper Surface of Noble Metal Nanostructure* (Univ Shandong, 2014).
[7]L. Si *et al.*, "Fabrication of one-dimensional $SnO_2$/$MoO_3$/C nanostructure assembled of stacking $SnO_2$ nanosheets from its heterostructure precursor and its application in lithium-ion batteries," J. Mater. Chem. A **2**(25), 9784–9791 (2014).
[8]J. Xie *et al.*, "Preparation of three-dimensional hybrid nanostructure-encapsulated sulfur cathode for high-rate lithium sulfur batteries," J. Power Sources **253**, 55–63 (2014).
[9]J. Hosseini *et al.*, "Electrocatalytic activity of porous nanostructured Fe/Pt-Fe electrode for methanol electrooxidation in alkaline media," Chin. J. Catal. **36**(7), 1029–1034 (2015).
[10]T. Wei *et al.*, "A high power density solid oxide fuel cell based on nanostructured $La_{0.8}Sr_{0.2}Cr_{0.5}Fe_{0.5}O_3$-$\delta$ anode," Electrochim. Acta **148**, 33–38 (2014).
[11]K. Wen *et al.*, "Interfacial strain effect on gas transport in nanostructured electrodes of solid oxide fuel cells," J. Power Sources **291**, 126–131 (2015).
[12]K. Zhu *et al.*, "Enhanced performance of solid oxide fuel cells by introducing a transition layer between nanostructured cathode and electrolyte," Int. J. Hydrogen Energy **40**(1), 501–508 (2015).
[13]N. Arun *et al.*, "Nanostructured spinel $LiNi_{0.5}Mn_{1.5}O_4$ as new insertion anode for advanced Li-ion capacitors with high power capability," Nano Energy **12**, 69–75 (2015).
[14]V. C. Bose and V. Biju, "Structure, cation valence states and electrochemical properties of nanostructured $Mn_3O_4$," Mater. Sci. Semicond. Process. **35**, 1–9 (2015).
[15]W. Lu *et al.*, "High performance electrochemical capacitors from aligned carbon nanotube electrodes and ionic liquid electrolytes," J. Power Sources **189**(2), 1270–1277 (2009).
[16]V. Augustyn *et al.*, "High-rate electrochemical energy storage through $Li^+$ intercalation pseudocapacitance," Nat. Mater. **12**(6), 518–522 (2013).
[17]J. Park, W. Lu, and A. M. Sastry, "Numerical simulation of stress evolution in lithium manganese dioxide particles due to coupled phase transition and intercalation," J. Electrochem. Soc. **158**(2), A201–A206 (2011).
[18]A. Daneyko *et al.*, "From random sphere packings to regular pillar arrays: Effect of the macroscopic confinement on hydrodynamic dispersion," J. Chromatogr. A **1218**(45), 8231–8248 (2011).

[19]R. S. Farr, "Random close packing fractions of lognormal distributions of hard spheres," Powder Technol. **245**, 28–34 (2013).
[20]P. Langston and A. R. Kennedy, "Discrete element modelling of the packing of spheres and its application to the structure of porous metals made by infiltration of packed beds of NaCl beads," Powder Technol. **268**, 210–218 (2014).
[21]L. Meng, P. Lu, and S. Li, "Packing properties of binary mixtures in disordered sphere systems," Particuology **16**, 155–166 (2014).
[22]K. D. L. Kristiansen, A. Wouterse, and A. Philipse, "Simulation of random packing of binary sphere mixtures by mechanical contraction," Phys. A: Stat. Mech. Appl. **358**(2–4), 249–262 (2005).
[23]S. R. Williams and A. P. Philipse, "Random packings of spheres and spherocylinders simulated by mechanical contraction," Phys. Rev. E **67**(5), 051301 (2003).
[24]J. G. Berryman, "Random close packing of hard spheres and disks," Phys. Rev. A **27**(2), 1053–1061 (1983).
[25]R. D. Groot and S. D. Stoyanov, "Close packing density and fracture strength of adsorbed polydisperse particle layers," Soft Matter **7**(10), 4750–4761 (2011).
[26]J. Crank, *The Mathematics of Diffusion* (Oxford Science Publications, Oxford [England], Clarendon Press, 1975).
[27]J. Song and M. Z. Bazant, "Effects of nanoparticle geometry and size distribution on diffusion impedance of battery electrodes," J. Electrochem. Soc. **160**(1), A15–A24 (2013).
[28]J. H. Lee *et al.*, "Effect of lithium powder size on the performance of lithium-powder/lithium trivanadate secondary batteries shown via impedance analysis," Electrochim. Acta **131**(0), 202–206 (2014).
[29]A. Adolph and M. R. Albert, "An improved technique to measure firn diffusivity," Int. J. Heat Mass Transf. **61**, 598–604 (2013).
[30]J. Liu *et al.*, "Characterization and electrochemical properties of $Li_2MoO_4$ modified $Li_4Ti_5O_{12}$/C anode material for lithium-ion batteries," Electrochim. Acta **170**, 202–209 (2015).
[31]C. Wang *et al.*, "Electrochemical properties of α-$MoO_3$-coated $Li[Li_{0.2}Mn_{0.54}Ni_{0.13}Co_{0.13}]O_2$ cathode material for Li-ion batteries," Electrochim. Acta. **176**, 1171–1181 (2015).
[32]D. Y. W. Yu *et al.*, "Electrochemical characterization of novel layered $Cu_2MS_4$ materials for Li-ion batteries (M = Mo)," Electrochim. Acta. **115**, 337–343 (2014).
[33]S. M. Zhang *et al.*, "Li ion diffusivity and electrochemical properties of $FePO_4$ nanoparticles acted directly as cathode materials in lithium ion rechargeable batteries," Electrochim. Acta. **88**, 287–293 (2013).
[34]S. Manzetti and F. Mariasiu, "Electric vehicle battery technologies: From present state to future systems," Renewable Sustainable Energy Rev. **51**, 1004–1012 (2015).
[35]J. Y. Yong *et al.*, "A review on the state-of-the-art technologies of electric vehicle, its impacts and prospects," Renewable Sustainable Energy Rev. **49**, 365–385 (2015).